International Tables for Crystallography (2018). Vol. H, Section 2.4.1, pp. 102–103.

2.4. Electron powder diffraction

J.-M. Zuo, J. L. Lábár, J. Zhang, T. E. Gorelik and U. Kolb

2.4.1. Introduction

Electron powder diffraction is commonly performed in transmission geometry inside a transmission electron microscope using ∼80–300 kV high-energy electrons with wavelengths from 0.0418 to 0.0197 Å (Cowley, 1992; Peng *et al.*, 2004). The incident electron beam can be as small as a few nm or as large as tens of μm in diameter. Transmission electron powder diffraction can be obtained from randomly oriented nanocrystalline or amorphous materials. The short electron wavelengths allow the observation of powder diffraction rings over a large range of S (= $\sin\theta/\lambda$). Electron powder diffraction can also be performed using the Bragg reflection geometry in reflection high-energy electron diffraction (RHEED) with 10–30 kV electrons (Ichimiya & Cohen, 2004). RHEED has a limited penetration depth and therefore is mostly used for the study of supported nanoparticles.

Because the electron beam can be formed into a small probe using electromagnetic lenses in a transmission electron microscope, electron diffraction has the advantage of being able to address individual particles in a powder as single crystals. Single-crystal electron diffraction data are often used for the determination of unit-cell parameters (Zuo, 1993; Zuo *et al.*, 1998; Gramm *et al.*, 2006; Sun *et al.*, 2009; Kolb *et al.*, 2006; Zhuang *et al.*, 2011), phase identification (Gramm *et al.*, 2006) or quantitative structural analysis (Vincent & Exelby, 1991; Jansen *et al.*, 1998; Tsuda & Tanaka, 1999; Hovmoller *et al.*, 2002; Sun *et al.*, 2009; Gorelik *et al.*, 2010; Mugnaioli *et al.*, 2012), or in combination with X-ray and neutron powder diffraction for structure determination (Wu *et al.*, 2006; Baerlocher *et al.*, 2007; McCusker & Baerlocher, 2009).

The principle of electron diffraction is similar to that of X-ray diffraction. Both use atomic scattering and interference of the scattered waves to probe the atomic structure. The difference is that electrons are charged particles and interact with both the electrons and nucleus of the atom with a large elastic scattering cross section (several orders of magnitude larger than that of X-rays). The combination of short wavelength, the large scattering cross section and the small electron beam makes electron powder diffraction a powerful technique for the analysis of amorphous or nanocrystalline thin films, nanoparticles and 'small' crystals in general (see Fig. 2.4.1 for an example).

A drawback of the strong interaction of electrons with matter is the presence of multiple-scattering effects. In X-ray diffraction, the measured integrated intensity is often less than predicted by the theory for an ideally imperfect crystal (because of extinction) but larger than predicted by the theory for an ideal perfect crystal. There are two types of extinction: primary and secondary. Primary extinction describes the multiple scattering within a single mosaic block. Primary extinction diminishes the intensity when the mosaic blocks are so large that they behave as fragments of perfect crystals. The effect of electron multiple scattering is similar to primary extinction in X-ray diffraction, except the electron extinction length is short and comparable with the sample thickness. Strong extinction can be an issue when analysis based on kinematical diffraction (single-scattering) theory, as in X-ray powder diffraction, is used for electron diffraction intensities; thus dynamic theory, which takes into account multiple scattering of the incident and diffracted waves inside a crystal, is necessary. Secondary extinction also occurs in electron powder diffraction. However, so far there is no satisfactory treatment of this effect in electron diffraction. For small nanoparticles or nanocrystalline thin films the electron multiple-scattering effects are typically reduced, so quantitative structural information can be extracted from electron powder diffraction using the kinematical approximation (Cockayne & McKenzie, 1988; Ishimaru *et al.*, 2002; Chen & Zuo, 2007; Cockayne, 2007). Recent studies have demonstrated that multiple-scattering effects can be significantly reduced by averaging over a range of crystal orientations using precession electron diffraction (Vincent & Midgley, 1994; Gjonnes *et al.*, 1998; Gemmi *et al.*, 2003; Own *et al.*, 2006; Oleynikov & Hovmoller, 2007). The same benefit is expected in electron powder diffraction with 360° orientation averaging.

The quality of electron powder diffraction work has also benefited from the development of TEM (transmission electron microscopy) technologies. The adoption of field emission guns (FEGs) in conventional transmission electron microscopes led to the development of electron sources with high brightness, small probe size and improved coherence. Electron energy filters, such as the in-column Ω energy filter, allow a reduction of the inelastic background due to plasmon scattering, or higher electron energy losses, with an energy resolution of a few eV (Rose & Krahl, 1995). The development of array detectors, such as charge-coupled device (CCD) cameras or image plates, enables the recording of entire powder diffraction patterns and direct quantification of diffraction intensities over a large dynamic range that was not possible earlier (Zuo, 2000). The latest

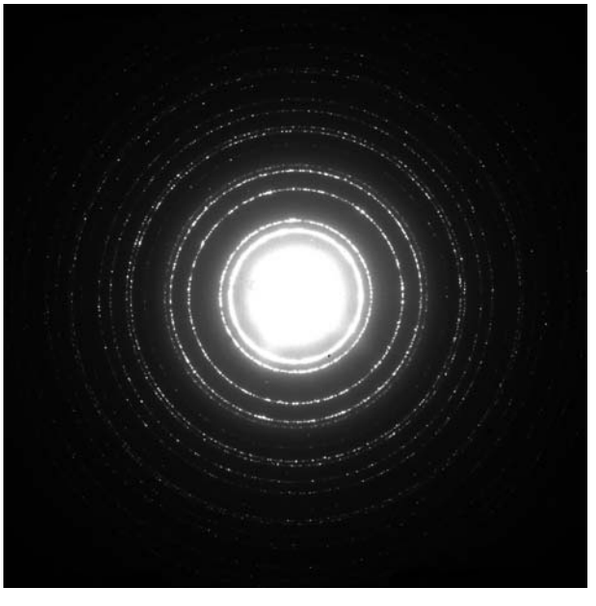

Figure 2.4.1
An electron powder diffraction pattern recorded on an imaging plate from a polycrystalline Al thin film using selected-area electron diffraction geometry with 200 kV electrons.

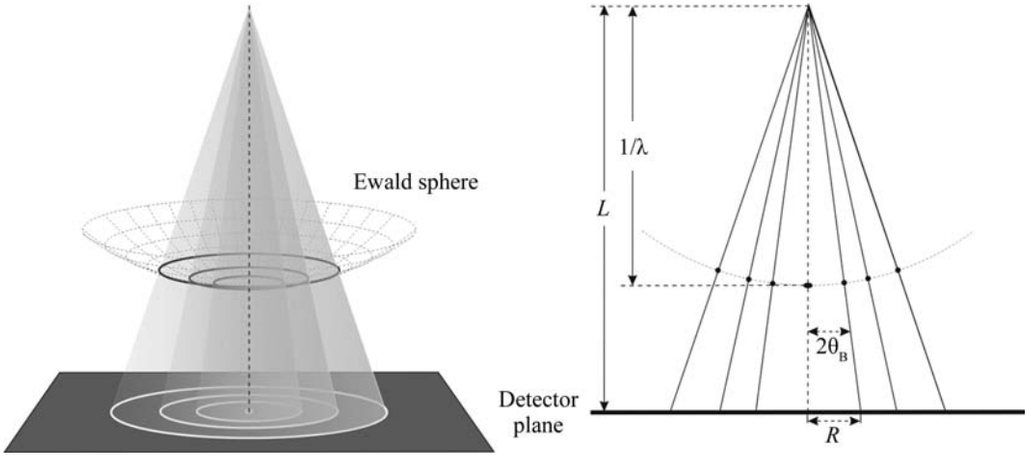

Figure 2.4.2
Schematic diagram of the Ewald sphere construction and the geometry for recording electron diffraction patterns.

development in time-resolved electron diffraction at a time resolution approaching femtoseconds (Elsayedali & Herman, 1990; Siwick *et al.*, 2003) will significantly improve the ability to interrogate structures at high spatial and time resolution.

Irradiation of both organic and inorganic materials with an electron beam can cause severe modification of the structure. The amount of energy deposited into the material can be estimated through the ratio of the elastic and inelastic scattering cross sections. For carbon the ratio for electrons (300 keV) and X-rays (with a wavelength of less than 1 Å) is comparable, meaning that the radiation damage caused by these sources is on the same scale (Henderson, 1995). Electron radiation damage is caused by all kinds of ionization processes, including bond breakdown and subsequent recombination of radicals and active molecular species. Inorganic materials can show knock-on damage (atomic displacement) or sputtering effects (loss of atoms). This damage may lead to a total structural collapse. The collective damage due to electron radiation is quantified using the electron dose and electron dose rates. In many cases the damage can be reduced by minimizing the electron dose received by the sample, cryo-protection, or deposition of a protective conductive layer (Reimer & Kohl, 2008).

This chapter covers the practical issues and theory of electron powder diffraction as well as applications for material analysis. A fundamental description of electron diffraction can be found in *International Tables for Crystallography*, Vol. C (2004) and the book by Zuo & Spence (2017). The present chapter is subdivided into seven sections. Sections 2.4.2 and 2.4.3 cover the theory and the experimental setup of an electron powder diffraction experiment using transmission electron microscopes, respectively. Sections 2.4.4 and 2.4.5 discuss the application of electron powder diffraction data to phase and texture analysis and related techniques. Rietveld refinement with electron powder diffraction data is a relatively new field; this is discussed in Section 2.4.6. The last section reviews pair distribution function (PDF) analysis using electron diffraction data.

2.4.2. Electron powder diffraction pattern geometry and intensity

By J.-M. Zuo and J. L. Lábár

The powder diffraction rings in transmission geometry appear where the cone of diffracted electron beams intersects the Ewald sphere. The intersection creates a ring of diffracted beams, which is then projected onto the planar detector (see Fig. 2.4.2) with a radius (R) according to

$$R = L \tan 2\theta_{\rm B}. \tag{2.4.1}$$

Here $\theta_{\rm B}$ is the Bragg diffraction angle and L is the camera length.

The d-spacing can be obtained by measuring the length of R in an experimental diffraction pattern using

$$d = \frac{\lambda}{2 \sin \theta_{\rm B}}. \tag{2.4.2}$$

The electron wavelength is determined by the electron accelerating voltage (Φ), in volts:

$$\lambda = \frac{h}{(2m_e\Phi)^{1/2}} \simeq \frac{1.226}{[\Phi(1 + 0.97845 \times 10^{-6}\Phi)]^{1/2}}. \tag{2.4.3}$$

The wavelength of high-energy electrons is relatively short. For 200 kV electrons, the wavelength is 0.025 Å and the Bragg angle is very small. For example, for d = 2.5 Å the electron scattering angle θ is 5 mrad. For a small Bragg angle one can use the approximation $\sin\theta \simeq \tan\theta \simeq \theta$. This gives the relationship

$$d \simeq \frac{L\lambda}{Rd}. \tag{2.4.4}$$

At large scattering angles with $\sin\theta/\lambda$ 2 Å^{-1} or greater, a better approximation is given by (Cowley & Hewat, 2004)

$$d \simeq \frac{L\lambda}{R}\left(1 + \frac{3R^2}{8L^2}\right). \tag{2.4.5}$$

The camera length L can be determined using a sample with known d-spacings, while the electron wavelength or acceleration voltage can be calibrated using high-order Laue zone (HOLZ) lines in convergent-beam electron diffraction (CBED) patterns (Zuo, 1993).

For a small parallelepiped crystal fully illuminated by a coherent electron beam of intensity I_0, the kinematic diffraction intensity is given by

$$I_{\rm SC} = I_0 \frac{\left|F_{hkl}\right|^2}{L^2}\left\{\frac{\sin[\pi\mathbf{S}_{hkl}\cdot N_1\mathbf{a}]}{\sin[\pi\mathbf{S}_{hkl}\cdot\mathbf{a}]}\frac{\sin[\pi\mathbf{S}_{hkl}\cdot N_2\mathbf{b}]}{\sin[\pi\mathbf{S}_{hkl}\cdot\mathbf{b}]}\frac{\sin[\pi\mathbf{S}_{hkl}\cdot N_3\mathbf{c}]}{\sin[\pi\mathbf{S}_{hkl}\cdot\mathbf{c}]}\right\}^2, \tag{2.4.6}$$

where N_1, N_2 and N_3 are the number of unit cells along the three axis directions, and F_{hkl} is the electron structure factor of the hkl reflection:

references